Available online at www.sciencedirect.com
SCIENCE DIRECT®
Journal of Magnetic Resonance 171 (2004) 4–9
JMR Journal of Magnetic Resonance
www.elsevier.com/locate/jmr

A simple method to measure $^{13}CH_2$ heteronuclear dipolar cross-correlation spectral densities

Djaudat Idiyatullin, Vladimir A. Daragan, Kevin H. Mayo*

Department of Biochemistry, Molecular Biology and Biophysics, University of Minnesota Health Science Center, 321 Church Street, Minneapolis, MN 55455, USA

Received 28 January 2004; revised 11 May 2004
Available online 24 August 2004

Abstract

Here, we report a method to simultaneously determine CH_2 cross-correlation spectral densities and T_1 relaxation times in the laboratory and rotating frames. To accomplish this, we have employed an indirect approach that is based on measurement of differences in relaxation rates acquired with and without cross-correlation terms. The new method, which can be employed using multidimensional NMR and standard relaxation pulse sequences, is validated experimentally by investigation of a selectively ^{13}C-enriched hexadecapeptide and the uniformly ^{13}C-enriched immunoglobulin-binding domain of streptococcal protein G (GB1). Use of this approach makes determination of CH_2 cross-correlation spectral densities in uniformly ^{13}C-enriched proteins now routine and provides novel information concerning their internal motions.

Keywords: Cross-correlations; NMR relaxation

1. Introduction

Cross-correlation spectral densities $J_{ab}(\omega)(a \neq b)$ describing mutual motions of the motional vectors a and b, for example the C–H groups in a methylene, provide unique information about internal motions in molecules. However, despite various publications related to dipolar and dipolar-CSA cross-correlations, these relaxation terms are not generally used. The main reason for this rests primarily in the fact that existing methods to measure cross-correlation effects are complicated and exhibit relatively low sensitivity. In addition, NMR relaxation theory of cross-correlation effects is quite complicated, making their interpretation difficult. Here, we report a relatively simple NMR method to measure heteronuclear dipolar cross-correlation terms, as well as some simple equations to interpret cross-correlation data.

The cross-correlation spectral density $J_{ab}(\omega)$ is defined as:

$$J_{ab}(\omega) = 4\pi_0 \int_0^\infty Y_{20}(\Omega_a(t)) Y_{20}(\Omega_b(0)) > \cos(\omega t)\,\mathrm{d}t, \quad (1)$$

where Ω_a and Ω_b denote polar angles θ and ϕ for motional vectors a and b in the laboratory frame, and Y_{20} is the spherical harmonic function. If internal molecular motions are approximated by a single correlation time, τ_i^*, then $J_{ab}(\omega)$ is described by a Lipari–Szabo type equation [1,2]:

$$J_{ab}(\omega) = S_{ab}^2 \frac{\tau_0}{1+\omega^2\tau^2} + \left(P_2(\cos\Theta) - S_{ab}^2\right)\frac{\tau_i}{1+\omega^2\tau^2}, \quad (2)$$

where $1/\tau_i = 1/\tau_i^* + 1/\tau_o$, τ_o, is the overall tumbling correlation time, θ_{ab} is the angle between the vectors a and

* Corresponding author. Fax: +1 612 624 5121.
E-mail address: mayox001@umn.edu (K.H. Mayo).

1090-7807/$ - see front matter © 2004 Elsevier Inc. All rights reserved.
doi:10.1016/j.jmr.2004.06.019

b, and $P_2(x) = 0.5\,(3x^2 - 1)$. The Lipari–Szabo equation can be easily obtained from Eq. (2) by using $\theta_{ab} = 0$.

The cross-correlation order parameter, S^2_{ab}, strongly depends upon motional restrictions. For fully restricted internal motions (rigid molecule) in a tetrahedron, $S^2_{ab} = -1/3$. For free rotation about an axis making a tetrahedral angle with vectors a and b (e.g., rotation of the methyl group where a and b are the C–H bonds), $S^2_{ab} = 1/9$. Therefore, the sign of S^2_{ab} indicates the degree of internal motional restriction—the more negative, the more restricted.

The standard, auto-correlation order parameter S^2_a is related to S^2_{ab}. This relationship depends on the rotational geometry of the group. For tetrahedral geometry where the angle between a and b and the angle between a, b and the rotation axis are all tetrahedral (typical for aliphatic chains), one can write [3]:

$$S^2_{ab} = 1/6 - S^2_a/2. \tag{3}$$

This equation is valid for restricted or unrestricted rotation about a single axis. In the case of unrestricted rotation, $S^2_{ab} = S^2_a = 1/9$ [2]. Deviation from Eq. (3) indicates that additional internal rotations, correlated fluctuations and/or overall motional anisotropy should be considered. These cases will be discussed later.

Another way to analyze cross-correlation data is to compare auto- and cross-correlation spectral density functions. Consider spectral densities $J_{\mathrm{CH}}(\omega)$ and $J_{\mathrm{CHCH'}}(\omega) = J_{\mathrm{HCH}}(\omega)$. While $J_{\mathrm{HCH}}(\omega_{\mathrm{c}})$ and $J_{\mathrm{HCH}}(0)$ can be determined directly from experiment by detecting three spin order (as will be demonstrated later), the auto correlation spectral density function $J_{\mathrm{CH}}(\omega)$ cannot. $J_{\mathrm{CH}}(\omega)$ is normally derived by using dipole–dipole ^{13}C spin–lattice relaxation rates, W_{C}, determined as a linear combination of these spectral densities as a function of the precession frequency:

$$W_{\mathrm{C}} = N\frac{\gamma_{\mathrm{C}}\gamma_{\mathrm{H}}\hbar^2}{r^6_{\mathrm{CH}}}J^*_{\mathrm{CH}}(\omega), \tag{4}$$

where N is the number of protons directly bonded to carbon; $\hbar^2$ is Planck's constant divided by 2π; γ_{C} and γ_{H} are the magnetogyric ratios for carbon and hydrogen nuclei, respectively, and r_{CH} is the internuclear distance. $J^*_{\mathrm{CH}}(\omega)$ is the linear combination of spectral densities

$$J^*_{\mathrm{CH}}(\omega) = 0.1(J_{\mathrm{CH}}(\omega_{\mathrm{C}} - \omega_{\mathrm{H}}) + 3J_{\mathrm{CH}}(\omega_{\mathrm{C}}) + 6J_{\mathrm{CH}}(\omega_{\mathrm{CH}} + \omega_{\mathrm{H}})). \tag{5}$$

The ratio $J_{\mathrm{HCH}}(\omega)/J^*_{\mathrm{CH}}(\omega)$ can serve as a good indicator for the time scale of internal motions. Fig. 1 plots $J_{\mathrm{HCH}}(\omega)/J^*_{\mathrm{CH}}(\omega)$ vs. the internal motional correlation time, τ_{i}, for various values of the auto-correlation order parameter S^2_{CH}. For this calculation, the overall tumbling correlation time, τ_0, is 5000 ps, and the cross-correlation order parameter, S^2_{HCH}, is related to S^2_{CH} by Eq. (3). A value of $S^2_{\mathrm{CH}} = 0.111$ corresponds to totally

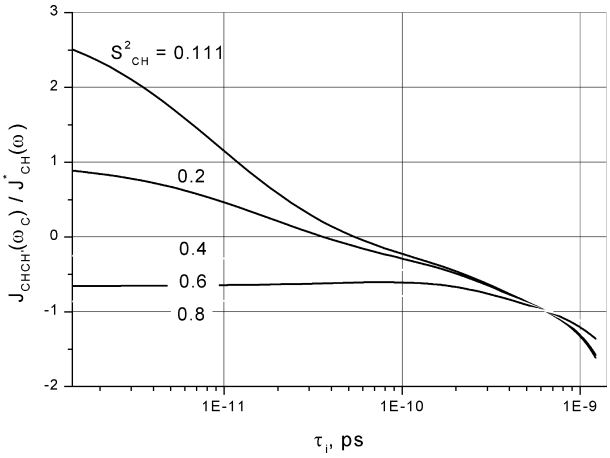

Fig. 1. Calculated ratios of auto- and cross-correlation spectral densities are plotted as a function of the internal motional correlation times τ_{i} for various values of the auto-correlation order parameter S^2_{CH}. In these calculations, the overall correlation time $\tau_0 = 5000$ ps. Tetrahedral geometry is assumed.

free rotation. From this plot, it is apparent that positive values of the ratio $J_{\mathrm{HCH}}(\omega)/J^*_{\mathrm{CH}}(\omega)$ are found only if the internal rotational correlation time is small and S^2_{CH} is less than 0.4.

For methylene groups in proteins (glycines and side-chains), the most important cross-correlation spectral density function is $J_{\mathrm{HCH}}(\omega)$, which can be used to indicate the character and geometry of internal motions. For glycines, $J_{\mathrm{HCH}}(\omega)$ values are particularly useful to discriminate backbone motions in more mobile regions that often play a key role in the biological activity of proteins. However, measuring cross-correlation terms from methylene groups in proteins is not a simple task. Aside from usually requiring selective, isotopic enrichment, the simplest method to measure $J_{\mathrm{HCH}}(\omega_{\mathrm{C}})$ is by inversion recovery relaxation experiments of ^{13}C multiplet spectra. In this case, $J_{\mathrm{HCH}}(\omega_{\mathrm{C}})$ is proportional to the difference between the initial relaxation rates of outer, W_{o}, and inner, W_{i}, lines of the ^{13}C triplet [2], as defined by

$$W_{\mathrm{o}} - W_{\mathrm{i}} = \frac{6}{5}\frac{\gamma_{\mathrm{C}}\gamma_{\mathrm{H}}\hbar^2}{r^6_{\mathrm{CH}}}J_{\mathrm{HCH}}(\omega_{\mathrm{C}}). \tag{6}$$

This method, however, cannot be used with large proteins, even in a multidimensional NMR version because of low sensitivity and resonance overlap. Brondeau et al. [4] and Ernst and Ernst [5] suggested unique methods to measure cross-correlation spectral densities that rely on cross-relaxation between $4S_zI_{1z}I_{2z}$ and S_z spin orders. Use of their methods generates a signal (with proton decoupling) that is proportional to the cross-correlation term and can be detected by 2D NMR techniques. However, these approaches have some drawbacks: (1) they require suppression of undesired terms like $\langle S_z\rangle$ before the relaxation delay interval at the beginning and end

of the mixing time, leading to substantial experimental error, (2) they yield very weak signals, and (3) they require the measurement of initial relaxation rates with $A(0) = 0$ in $A(t)$ curves. Errors in pulse widths and other factors can provide substantial error in determining these initial rates. Some of these problems can be avoided. For example, Daragan et al. [6] showed that measuring initial slopes $A(t)$ of the sum of exponential relaxation decays with non-zero initial values $A(0)$ can be performed more accurately, with the influence of a non-vanishing $\langle S_z \rangle$ term being greatly reduced. It would also be advantageous to be able to simultaneously measure cross-correlation and auto-correlation terms (like T_1), something that standard relaxation pulse sequences [7] cannot do.

In this paper, we report a method to determine cross-correlation spectral densities and T_1 relaxation times in the laboratory and rotating frames by using indirect approaches based on the measurement of differences in relaxation rates acquired with and without cross-correlation terms.

2. Methods and materials

Fig. 2 illustrates the pulse sequence used to measure simultaneously auto- and cross-correlation terms in the laboratory and rotating frames for CH_2 groups. During the recycle time, a 120° ^{1}H pulse train is applied to saturate ^{1}H magnetization. The following part of the pulse sequence is used to measure the spin–lattice relaxation rate via inversion-recovery with and without detection of cross-correlation terms. The first $90^\circ_x 90^\circ_\phi$ double pulse on the ^{13}C channel is applied where ϕ is alternately changed to make this pulse act like 180° or 0° pulses. After the 180°-like pulse, magnetization recovery is described as $A(1 - K_1\exp(-t/T_1))$, and after the 0°-like pulse, it is described as $A(1 - K_2\exp(-t/T_1))$. The difference from these decay curves, which is easily derived by receiver phase alternating, is given by a single exponential that can be fit by two parameters.

During the interval T, C_z magnetization decays and is partially transformed to three spin order $4C_zH_zH'_z$ due to dipole–dipole cross-correlation [2,5,8,9]. For CH_2 groups, $4C_zH_zH'_z$ is proportional to the difference between intensities of outer and inner lines of the ^{13}C multiplet. Upon removing three spin order, ^{13}C T_1 values are measured without the influence of cross-correlation. This is achieved by rotating H_z magnetization into the x,y plane by using a ^{1}H 90° pulse (p*), transforming spin order to $4C_zH_yH'_y$ that is not detectable. Without this pulse, relaxation terms with both one and three spin orders C_z and $4C_zH_zH'_z$, respectively, are present and are transferred identically by using the inverse INEPT sequence. As a result, one obtains a detectable relaxation decay signal having an initial rate

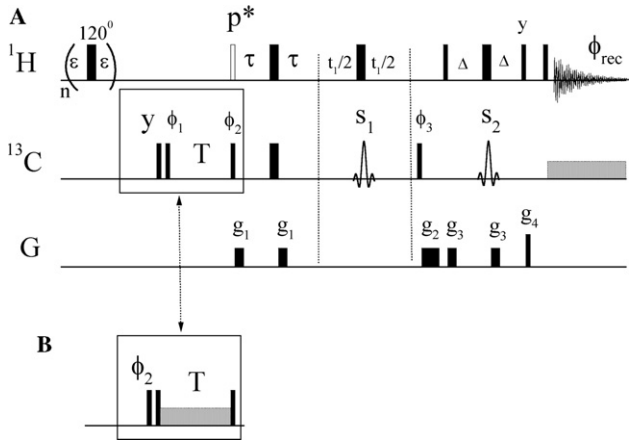

Fig. 2. Pulse sequences used for determining auto and cross-correlation rates in the laboratory (A) and rotating (A with insertion of B) frames for CH_2 groups are shown. 90° and 180° pulses are represented proportionally by the thickness of bars. Unless otherwise indicated, all pulses are applied along the X-axis. Proton irradiation is achieved by applying 120° pulses spaced at 5 ms ($\varepsilon = 2.5$ ms) intervals [13] during the repetition time of $5T_1$ in duration. Two sets of relaxation experiments with the same arrayed values are carried out with and without using the first H^1 90° pulse (open pulse on figure with $p^* = 90°$ or $p^*=0°$). Delays were set as follows: $\Delta \leqslant 1/4J_{CH}$, $\tau = 1/8J_{CH}$. The duration of all gradient pulses was 500 mks, except for the g_2 pulse duration which was set to 1 ms. Amplitudes of gradient pulses were: $g_1 = 4.28$ G/cm; $g_2 = 18$ G/cm; $g_3 = 3$ G/cm; and $g_4 = 21$ G/cm. Phase cycling was: $\phi_1 = 4(y),4(-y)$;$\phi_2 = 2(y,-y),2(-y,y)$; $\phi_3 = 2(x),2(-x)$; and $\phi_{rec} = x,-x,-x,x,-x,x,x,-x$. S_1 is a sine-shaped 180° pulse placed at CO resonance. S_2 is a selective hyperbolic secant 180° pulse [12] placed at the applied frequency.

equal to W_o—the relaxation rate of the outer lines of the ^{13}C multiplet. By using this pulse train during the recycle period, perturbing proton magnetization has no influence on the relaxation rate because the phase of the receiver is being alternated as mentioned previously.

By performing these two experiments as described above, one can obtain the relaxation rates W_o and W_C, as well as the cross-correlation spectral density. With $W_C = 1/T_1 = (W_o + W_i)/2$ for the CH_2 group, one obtains

$$W_o - W_C = \frac{3}{5}\frac{\gamma_C\gamma_H\hbar^2}{r_{CH}^6}J_{HCH}(\omega_C). \quad (7)$$

Maximal transfer of the outer components from the $^{13}CH_2$ multiplet is achieved at $\tau = 1/8J_{CH}$, where J_{CH} is the ^{1}H–^{13}C spin coupling constant.

In Fig. 2B, the pulse sequence to measure auto- and cross-correlation terms in the rotating frame is presented. Instead of having T_1, one obtains the value of $T_{1\rho}$ when the first 90° ^{1}H pulse is applied. Without this pulse, cross-correlation spectral densities contribute to the relaxation rate, and can be determined by using a modification of Eq. (7). As shown by Ernst and Ernst [5], one should express $J_{HCH}(\omega_C)$ in Eq. (7) as:

$$J_{\mathrm{HCH}}(\omega_C) \rightarrow \frac{1}{2}[(1+\cos^2\theta)J_{\mathrm{HCH}}(\omega_{\mathrm{C}}) + \frac{4}{3}\sin^2\theta J_{\mathrm{HCH}}(0)], \quad (8)$$

where

$$\cos^2\theta = \frac{\Delta\omega^2}{\Delta\omega^2 + \Delta\omega_{\mathrm{L}}^2} \quad (9)$$

$\Delta\omega$ is the frequency offset, and ω_{L} is the spin-lock frequency. The main difference between experiments performed in the laboratory and rotating frames is an additional term in Eq. (8), i.e., the cross-correlation spectral density at zero frequency. Performing these two experiments allows one to obtain values for $J_{\mathrm{HCH}}(\omega_{\mathrm{C}})$ and $J_{\mathrm{HCH}}(0)$, as well as for T_1 and $T_{1\rho}$.

To validate the use of this novel approach, we measured cross-correlation spectral densities in the laboratory and rotating frames using selectively ^{13}C-enriched glycine, G_{10}, in a collagen-based GXX-repeating hexadecapeptide GVKGDKGNPG_{10}WPGAPY [10] , and for all methylene groups in the fully ^{13}C-enriched 56-residue protein GB1 [11]. For comparison, the proven simple inversion recovery method for coupled ^{13}C spectra was used with the hexadecapeptide. Freeze-dried protein samples were dissolved in a D_2O at 10 mg/mL, and the pH was adjusted to pH 6 by adding microliter quantities of NaOD or DCl. NMR relaxation experiments were performed on Varian Inova-500, Inova-600 and Inova-800 NMR spectrometers equipped with triple-resonance probes. The temperature was set at 5 °C. Temperature calibration was done by using chemical shifts of resonances from methanol.

3. Results and discussion

Using the new approach, ^{13}C relaxation curves determined with and without cross-correlation effects are plotted as solid symbols in Fig. 3 for G_{10} in the hexadecapeptide. For comparison, relaxation curves from inner and outer lines of the ^{13}C multiplet from G_{10} in the hexadecapeptide, as determined using the standard inversion recovery method [6], are shown as open symbols. Note that the relaxation curve for the "proton-decoupled experiment" that measures W_{C} (new approach with data generated without cross-correlation, solid squares) falls between these relaxation curves as would be expected. Calculated values of cross-correlation spectral densities $J_{\mathrm{HCH}}(\omega_{\mathrm{C}})$ derived from these two experiments differ by less than 3%, validating use of the new approach to measuring cross-correlation terms.

Having validated the new approach, we next challenged it to assess cross-correlation effects from all methylene groups in the fully ^{13}C-enriched 56-residue protein

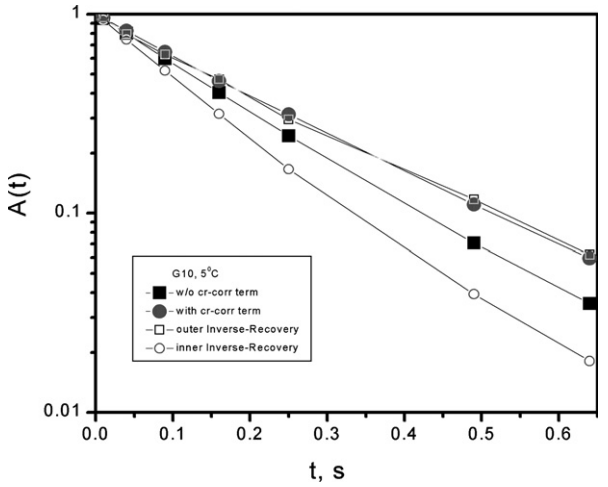

Fig. 3. Curves for multiplet ^{13}C relaxation of the methylene group of G10 in the collagen-based GXX-repeating hexadecapeptide GVKGDKGNPG_{10}WPGAPY [10] are shown. Open symbols indicate results from the inversion recovery experiment for the proton-coupled ^{13}C triplet. Filled symbols indicate results from the proton-coupled experiment described in the text.

GB1 [11]. Fig. 4 reports the ratio of $J_{\mathrm{HCH}}(\omega_{\mathrm{C}})/J^*_{\mathrm{CH}}(\omega)$ for methylene groups in GB1 at 5 °C. Data are shown for $\omega_{\mathrm{C}} = 150$ MHZ. The average value of this ratio for the four glycines (G9, G14, G38, and G41) in GB1 is -0.6 ± 0.3. Comparatively, a more negative value of this ratio is a relative indication of more restricted internal motion. Interestingly, this ratio is more negative for side-chain methylenes:

$$C_\beta H_2 : \langle J_{\mathrm{HCH}}(\omega_{\mathrm{C}})/J^*_{\mathrm{CH}}(\omega)\rangle = -0.87 \pm 0.5,$$

$$C_\gamma H_2 : \langle J_{\mathrm{HCH}}(\omega_{\mathrm{C}})/J^*_{\mathrm{CH}}(\omega)\rangle = -0.95 \pm 0.3,$$

Referring back to Fig. 1, one can conclude that internal motional correlation times for side-chain $C_\beta H_2$ and

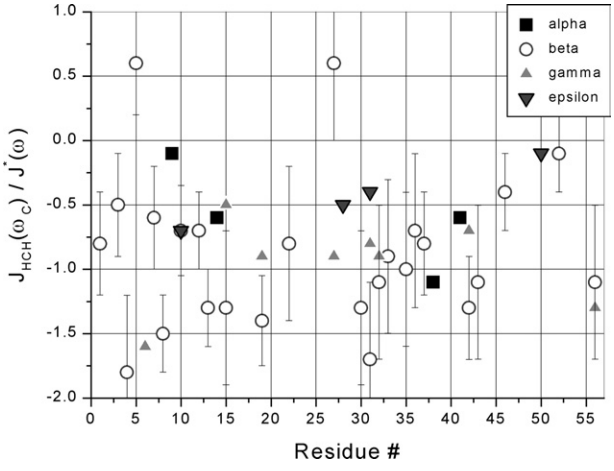

Fig. 4. The ratios of auto- and cross-correlation spectral densities for glycines and side chain methylene groups in GB1 are shown. Experimental error bars are shown for $C_\beta H_2$ methylene groups. For other methylene groups the errors are similar.

$C_\gamma H_2$ groups in GB1 are larger than for glycines in the backbone, indicating that side-chain internal motions are more restricted on average than those from backbone gylcine methylenes.

Fig. 5 shows the motional restriction map for all methylene groups in GB1 at 5 °C. A motional restriction map [2,3] plots the cross-correlation order parameter, S^2_{HCH}, vs. the auto-correlation order parameter, S^2_{CH}, for a given group and is presented in the context of various motional models, e.g., unrestricted rotation about a single axis, as well as restricted correlated and uncorrelated rotations, allowing insight into the types of motions for each methylene. For these calculations, the three Lorentzian model $J(\omega) = a_0 J_0(\omega) + a_1 J_1(\omega) + a_2 J_2(\omega)$ was used to calculate auto- and cross-correlation order parameters, which increased the accuracy of determining values of the order parameters. Here $a_0 = S^2$ (auto- or cross-correlation order parameter), $J_k(\omega) = \tau_k/(1 + \omega^2\tau_k^2)$, τ_0 is the overall correlation time, a_1, a_2 are some numerical coefficients, and $a_0 + a_1 + a_2 = P_2(\cos(\theta))$, where $P_2(x) = 0.5\ (3x^2 - 1)$ and $\theta = 0$ in case of auto-correlation function and θ is equal to the angle between CH bonds in case of cross-correlation. The minimization procedure was used to determine eight theoretical parameters $[\tau_0, \tau_1, \tau_2, a_0(\mathrm{CH}), a_1(\mathrm{CH}), a_0(\mathrm{HCH}), a_1(\mathrm{HCH}), R_{ex}]$ with 10 experimental parameters $[R_1, R_2, J_{HCH}(\omega_C)]$ at three frequencies and $J_{HCH}(0)$. Each point on the graph represents one methylene group, and all points on the graph lay inside the "triangle" formed by three curves. The upper left most linear curve describes unrestricted rotations about the C–C bond (as found for freely rotating methyl groups); the upper right most linear curve presents the limits for two fully negatively correlated rotations, and the curvi-linear bottom curve presents the limits for two fully positively correlated rotations [2].

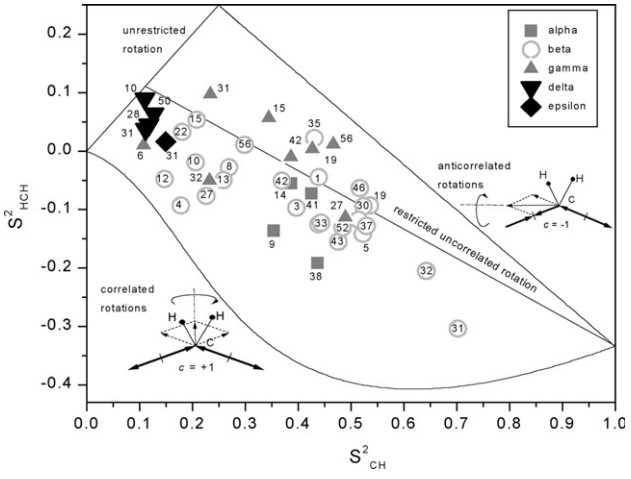

Fig. 5. A motional restriction map for glycines and side-chain methylene groups in GB1 is shown. Limiting curves are plotted for unrestricted, uncorrelated, and highly correlated rotations as indicated in the figure and discussed in the text.

The internal linear curve represents uncorrelated restricted rotations. For a glycine residue, rotations are restricted about N–C_α and/or C_α–C backbone bonds. For side chain methylene groups, C_iH_2, rotations are restricted rotations about C_{i-1}–C_i and/or C_i–C_{i+1} bonds. The equation describing these motions can be written as [2,3]:

$$S^2_{HCH} = \left(\frac{1}{6}\right)\left(1 - 3S^2_{CH}\right). \tag{10}$$

Two fully negatively correlated (anti-correlated) rotations are equivalent to rotation about the axis perpendicular to the HCH plane. In this case, the relationship between auto- and cross-correlation spectral densities can be written as [2,3]

$$S^2_{HCH} = \frac{4}{9} - \frac{7}{9}S^2_{CH}. \tag{11}$$

Equations describing positively correlated rotations are more complicated and computational modeling is required to describe them [2]. The two insets to Fig. 5 illustrate how these restricted, correlated motions may be envisioned. Negatively correlated motions lead to back-and-forth-like fluctuations of the H–C–H triangle as found for puckering-type motions in a proline ring [3]. Positively correlated motions lead to fluctuations about an axis bisecting the H–C–H triangle, like twisting-type motions [2]. Points lying between curves indicate more complicated combinations of these types of correlated fluctuations.

From Fig. 5, it is apparent that most $C_\gamma H_2$ groups tend to exhibit more negatively correlated rotations about their C_β–C_γ and C_γ–C_δ (and maybe also C_α–C_β) bonds, whereas most other methylene group motions are better described by positively correlated rotations. Two of the backbone glycines (G14 and G41) can be described by two independent $\phi(t)$ and $\psi(t)$ backbone rotations (restricted, yet uncorrelated); however, for G9 and G38 these motions are positively correlated. These types of motions for glycines may be correlated to specific constraints placed on the positions in which these particular residues are found in the structure of GB1. G9 and G38 are present in rather tight turns in GB1, whereas G14 and G41 are located within β-sheets.

It is also interesting to note that while internal motions of some methylene groups in smaller, less well-folded peptides are more restricted when plotted on this type of motional restriction map [14,15], some of those in both the core and surface of protein GB1 appear less restricted and more dispersed, covering a larger area through the restriction map. Although presently limited to comparison of GB1 and a few peptides (as opposed to the same methylene groups in an unfolded state of GB1), this observation suggests that the conformational entropy of certain side chains in GB1 may in fact be increased in the folded state relative to the unfolded state.

This idea runs contrary to the generally accepted view that conformational entropy (which can be derived from the order parameter S^2_{CH} [19–21]) of side chains is decreased (larger values of S^2_{CH} [19–21]) upon protein folding [16–18]. Protein folding may actually promote more varied and some less restricted types of internal motions. This and other hypotheses require further experimentation and analysis.

We conclude by stating that when viewing internal motions through the double lens of auto- and cross-correlation spectral densities, the finer details of side chain internal motions become more resolved. Because of this, recent interest in measuring and interpreting cross-correlation spectral densities, $J_{HCH}(\omega)$, in conjunction with auto-correlation spectral densities, has increased considerably [2,22–24]. Examples reported here indicate that employing this new NMR approach to measure auto- and cross-correlation motional parameters simultaneously is relatively straight forward and can be performed on proteins using multidimensional NMR.

Acknowledgments

This work was supported by a research grant from the National Institutes of Health (NIH, GM-58005) and benefited from use of the high field NMR facility at the University of Minnesota. NMR instrumentation was provided with funds from the NSF (BIR-961477), the University of Minnesota Medical School, and the Minnesota Medical Foundation. Computer resources were provided by the Minnesota Supercomputing Institute.

References

[1] G. Lipari, A. Szabo, Model-free approach to the interpretation of nuclear magnetic resonance relaxation in macromolecules. I. Theory and range of validity, J. Am. Chem. Soc. 104 (1982) 4546–4559.

[2] V.A. Daragan, K.H. Mayo, Motional model analyses of protein and peptide dynamics using ^{13}C and ^{15}N NMR relaxation, Prog. NMR Spectrosc. 32 (1997) 63–105.

[3] V.A. Daragan, K.H. Mayo, Using the model-free approach to interpret 13C NMR multiplet relaxation data from peptides and proteins, J. Magn. Reson. 107 (1995) 274–278.

[4] J. Brondeau, D. Canet, C. Millot, H.,Nery, L. Werbelow, The direct experimental determination of dipole–dipole cross-correlation spectral density, J. Chem. Phys. 82, 2212–2216.

[5] M. Ernst, R.R. Ernst, Heteronuclear dipolar cross-correlated cross-relaxation for the investigation of side-chain motions, J. Magn. Reson. A 110 (1994) 202–213.

[6] V.A. Daragan, M.A. Kloczewiak, K.H. Mayo, ^{13}C nuclear magnetic resonance relaxation-derived psi, phi bond rotational energy barriers and rotational restrictions for^{13}C alpha-methylenes in a GXX-repeat hexadecapeptide, Biochemistry 32 (1993) 10580–10590.

[7] V. Sklenar, D. Torchia, A. Bax, Measurement of carbon-13 longitudinal relaxation using^{1}H detection, J. Magn. Reson. 73 (1987) 375–379.

[8] L.G. Werbelow, D.M. Grant, Intramolecular dipolar relaxation in multispin systems, Adv. Magn. Reson. 9 (1977) 189.

[9] M.M. Fuson, J.H. Prestegard, Dynamic properties of malonic acid in solution from spin relaxation of a ^{13}C-labeled methylene group, J. Chem. Phys. 76 (1982) 1539–1549.

[10] V.A. Daragan, K.H. Mayo, ^{13}C-{^{1}H} NMR/NOE and multiplet relaxation data in modeling protein dynamics of a collagen ^{13}C-enriched glycine GXX repeat motif hexadecapeptide, J. Am. Chem. Soc. 114 (1992) 4326–4331.

[11] A.M. Gronenborn, D.R. Filpula, N.Z. Essig, A. Achari, M. Whitlow, P.T. Wingfield, G.M. Clore, A novel, highly stable fold of the immunoglobulin binding domain of streptococcal protein G, Science 253 (1991) 657–661.

[12] M.S. Silver, R.I. Joseph, D.I. Hoult, Selective spin inversion in nuclear magnetic resonance and coherent optics through an exact solution of the Bloch–Riccati equation, Phys. Rev. A 31 (1985) 2753–2755.

[13] J.L. Markley, W.J. Horsley, M.P. Klein, Spin–lattice relaxation measurement in slowly relaxing complex spectra, J. Chem. Phys. 53 (1971) 3604–3605.

[14] M. Ramirez-Alvarado, V.A. Daragan, L. Serrano, K.H. Mayo, Motional dynamics of residues in a β-hairpin peptide measured by ^{13}C-NMR relaxation, Protein Sci. 7 (1998) 720–729.

[15] D. Idiyatullin, A. Krusheknitsky, I. Nesmelova, F. Blanco, V.A. Daragan, L. Serrano, K.H. Mayo, Internal motional amplitudes and correlated bond rotations in an α-helix peptide derived from^{13}C- and ^{15}N-NMR relaxation, Protein Sci. 9 (2000) 2118–2127.

[16] G.I. Makhatadze, P.L. Privalov, Energetics of protein structure, Adv. Protein Chem. 47 (1995) 307–425.

[17] H.S. Chan, K.A. Dill, Protein folding in the landscape perspective: chevron plots and non-Arrhenius kinetics, Proteins: Struct. Funct. Genet. 30 (1998) 2–33.

[18] A.L. Lee, A.J. Wand, Microscopic origins of entropy, heat capacity and the glass transition in proteins, Nature 411 (2001) 501–504.

[19] M. Akke, R. Bruschweiler, A.G. Palmer III, NMR order parameters and free energy. An analytical approach and its application to cooperative Ca^{2+} binding by calbindin D9k, J. Am. Chem. Soc. 115 (1993) 9832–9833.

[20] D. Yang, L.E. Kay, Contributions to conformational entropy arising from bond vector fluctuations measured from NMR-derived order parameters: application to protein folding, J. Mol. Biol. 263 (1996) 369–382.

[21] D. Idiyatullin, V.A. Daragan, K.H. Mayo, Heat capacities and a snapshot of protein GB1 energy landscape from the temperature dependence of backbone NH nanosecond fluctuations, J. Mol. Biol. 325 (2003) 149–162.

[22] M.W.F. Fischer, A. Majumdar, E.R.P. Zuiderweg, Protein NMR relaxation: theory, applications and outlook, Prog. Nucl. Magn. Reson. Spectrosc. 33 (1998) 207–272.

[23] B. Brutscher, Principles and applications of cross-correlated relaxation in biomolecules, Concept Magn. Reson. 12 (2000) 207–229.

[24] A. Kumar, R. Christy, R. Grace, P.K. Madhu, Cross-correlations in NMR, Prog. Nucl. Magn. Reson. Spectrosc. 37 (2000) 191–319.